Biochimica et Biophysica Acta, 1100 (1992) 125–136

BBABIO 13603

The structure of Photosystem I from the thermophilic cyanobacterium *Synechococcus* sp. determined by electron microscopy of two-dimensional crystals

Bettina Böttcher [a,b], Peter Gräber [b] and Egbert J. Boekema [a]

[a] *BIOSON Research Institute, University of Groningen, Groningen (Netherlands) and* [b] *Biologisches Institut, Universität Stuttgart, Stuttgart (Germany)*

(Received 8 October 1991)
(Revised manuscript received 3 February 1992)

Key words: Photosystem I structure; Electron microscopy; (Cyanobacteria)

The structure of the Photosystem I (PS I) complex from the thermophilic cyanobacterium *Synechococcus* sp. has been investigated by electron microscopy and image analysis of two-dimensional crystals. Crystals were obtained from isolated PS I by removal of detergents with Bio-Beads. After negative staining, either single layers or two superimposed layers with a rotational different orientation were observed. The layers have a rectangular unit cell of 16.0 × 15.0 nm, which contains two PS I monomers. The monomers are arranged alternating up and down in each layer. For double-layer crystals, the images of the two layers could be separately processed by a combination of Fourier-peak-filtering and correlation averaging. Features in the two-dimensional plane can be seen with a resolution up to 1.5–1.8 nm. A model for the PS I structure was obtained by combining three-dimensional reconstructions from three tilt-series. The model shows an asymmetric PS I complex. On one side (presumably the stromal side) there is a 3 nm high ridge. This is most likely comprised of the psaC, psaD and psaE subunits. The other side (presumably the lumenal side) is rather flat, but in the center there is a 3 nm deep indentation, which possibly separates partly the two large subunits psaA and psaB.

Introduction

The Photosystem I (PS I) complex catalyzes the light-dependent transfer of electrons from reduced plastocyanin or cytochrome *c*-553 to soluble ferredoxin. It is an abundant constituent of the photosynthetic membranes from green plants and cyanobacteria. PS I consists of two high molecular mass subunits of about 83 kDa (psaA and psaB) which are very hydrophobic and bind most, if not all, of the 60–100 chlorophylls associated with the PS I complex. A large number of subunits with a mass under 20 kDa (named psaC, psaD to psaO) is present with one copy [1]. Higher plant PS I appears to contain 11 different small subunits (psaC, psaD, -E, -F, -I, -J, -K, -L and -O) and cyanobacterial PS I contains about 9 small subunits (psaC, -D, -E, -F, -I, -J, -K, -L and -M); (see Refs. 1–4) for reviews). Photoexcitation of one of the antenna chlorophylls leads to a charge separation between the primary electron donor, P-700 and the primary electron acceptor, A_0. The electron then passes through intermediate acceptors A_1 and F_X to the terminal acceptors F_B and F_A. The identity of these electron transport components is known: P-700 is probably a chlorophyll dimer, A_0 is a chlorophyll monomer, A_1 is most likely phylloquinone (vitamin K_1), and F_X, F_A and F_B are iron-sulfur clusters [1–4].

PS I has been purified from thermophilic cyanobacteria by several groups [5–9]. The low-resolution structure of PS I has been studied by electron microscopy of single particles [10–12] and two-dimensional crystals [13]. High-resolution structure determination by X-ray diffraction is in progress [14–17].

Crystallization into two-dimensional sheets has been very helpful to solve the low- and high-resolution structure of isolated membrane proteins. About 20 objects have been studied in this way. The three-dimensional structure of bacteriorhodopsin has been solved recently to a resolution high enough to see the individual amino-acid side-chains [18].

Correspondence: E.J. Boekema, BIOSON Research Institute, University of Groningen, Nijenborgh 4, 9747 AG Groningen, The Netherlands.

Ways of obtaining two-dimensional crystals of isolated membrane proteins have been described (reviewed in [19]). In one method, the isolated protein is reconstituted in a phospholipid bilayer with a high protein to lipid ratio. During reconstitution excessive detergent- and lipid molecules are removed by dialysis or by adsorption with Bio-Beads. As a result, lipid bilayers in the form of sheets or vesicles with ordered protein molecules are obtained. Once the bilayers are formed, ordering of the protein molecules can be enhanced by incubation with (phospho)lipases which break down excess of lipid. In this way we have obtained crystals from the purified cyanobacterial PS I complex. Here we present image analysis of the two-dimensional projections of the PS I crystals and the three-dimensional reconstruction from filtered projections of tilted crystals.

Materials and Methods

Cells of the thermophilic cyanobacterium *Synechococcus* sp. [9,10] were a gift of Prof. H.T. Witt. About 100 g of cells were washed with buffer 1 (20 mM Na-Mes (pH 6.5), 10 mM $CaCl_2$, 10 mM $MgCl_2$). The pellets were resuspended in 200 ml of the same buffer to which 500 mM mannitol and 200 mg lysozyme (183000 U/mg dissolved in 5 ml of the same buffer) were added. The resulting protoplasts were centrifuged at $17000 \times g$ for 10 min and osmotically shocked in 300 ml of buffer 1. The membranes were collected by 10 min centrifugation at $17000 \times g$ and resuspended in 300 ml buffer (10 mM Na-Mes (pH 6.0), 100 mM NaCl). This washing procedure was repeated (about 5–15 times) until the phycobilisomes were removed (i.e., the blue color of the supernatant disappeared). Finally, the pellets were washed twice with 10 mM Mes pH 6.0 and resuspended in the same buffer so that a maximum of 50 ml was obtained. Then, 50 ml solubilization medium was added (38 mM octyl glucoside, 28 mM dithiothreitol, 16 mM sodium cholate) and the mixture was incubated at 4°C for 30 min, followed by centrifugation for 60 min at $50000 \times g$. The protein obtained from the supernatant was fractionated by ammonium sulfate precipitation (20%, 35% and 50%). Pellets from the 50% fraction were resuspended in the gradient medium without sucrose. In this solution, the protein extract can be frozen and stored in liquid nitrogen until use. For purification, the extract was layered on a sucrose density gradient (steps 12%, 18%, 23%, 26%, 28%, 30%, 40%) using a gradient medium which contained 30 mM Tris-succinate pH 6.5, 0.5 mM EDTA, 0.2% Triton X-100 and 0.2 mM ATP. After centrifugation in a Beckman Vac50 rotor for 16 h at $107000 \times g$ (4°C), Photosystem I was found between 30 and 40% steps (sometimes directly as crystalline sheets) as well as in the 40% step. In some cases, the solubilization was carried out with 0.4% sulfobetain 12 under the same conditions as described above. In this case, PS I was obtained from the pellets after sucrose gradient centrifugation was done.

The subunit composition of PS I was determined by SDS-gel electrophoresis with the Phast System (Pharmacia). Before gel electrophoresis the 30–40% fraction from the sucrose density gradient was subjected to HPLC on a Mono Q column (Pharmacia) and eluted with a linear $MgSO_4$ gradient (25–200 mM). The elution pattern indicates that the sample contains mainly PS I monomers and additionally some PS I trimers and PS II and H^+-ATPase as impurities. The PS I containing peak was used for gel electrophoresis. For obtaining the two-dimensional crystals this additional purification was not necessary.

Two-dimensional crystals were prepared by treatment of 20 μl aliquots of isolated PS I with about 5–10 beads of Bio-Beads SM 7 (Bio-Rad) and 0.5–1 units of phospholipase A_2 (from *Naja mossambique*, Sigma) or 10 units of lipase (Type VII from *Candida cylindracea*, Sigma) at 4°C between 3–14 days.

For electron microscopy, aliquots of the crystalline material were prepared using the droplet method with 1% uranyl acetate as negative stain. During the staining procedure the grid was washed about 5–10 times with 1% uranyl acetate in order to remove most of the sucrose. Electron microscopy was performed with a Philips EM 400 electron microscope. Micrographs used for the analysis were taken with 80 kV at $60000\times$ magnification. Care was taken not to preilluminate the part of the specimen to be recorded, to avoid excessive specimen damage. Metal shadowing experiments were carried out with an Edwards evaporating device at room temperature at a vacuum of 10^{-5} torr.

Selected micrographs were digitized with a Joyce-Loebl Scandig 3 rotating drum densitometer or with an Eikonix Model 1412 CCD camera equipped with a Nikon objective lens (AF Micro Nikkor, focal length 105 mm). A step size of 25 μm, corresponding to a pixel (image element) size of approx. 0.42 nm at the specimen level was used. Image analysis was carried out on a Convex C1-XP mini-supercomputer using IMAGIC software.

Two-dimensional crystalline arrays were processed by a combination of Fourier-peak filtering and correlation averaging [21]. Crystalline areas were divided into 128×128 pixel fragments. The first reference for alignment of the fragments was made by Fourier-peak filtering of a 1024×1024 transform. In the case of double layer crystals both layers could be separated using different masks on the Fourier transform [22]. The peaks were found with a peak search program using least-square fitting of a parabolic curve over the peaks. The alignment of the fragments was performed with correlation methods and was repeated several

times. Finally, the best 50% of the fragments were summed with the correlation coefficient as a quality measure.

A three-dimensional model was obtained by combining the results from three reconstructions from three different single-axis tilt series. A direct-space iterative algorithm was used [23,24]. The method included the following steps:

(1) Each of the two-dimensional projections was filtered by the combination of Fourier-peak filtering and correlation averaging.

(2) The common origin in the averaged 128×128 pixel projections of each tilt series was determined by calculating the translational cross-correlation function between subsequent members of the series, using the untilted image as starting point.

(3) The direction of the tilt axis was determined and the angle of tilt was checked by comparing the calculated unit-cell dimensions in the tilted and untilted projections [25].

(4) The thus aligned 128×128 pixel projections of each tilt series were used to calculate the three-dimensional reconstruction. In the first reconstructions we took the whole filtered projection and reconstructed the crystal in a $128 \times 128 \times 128$ pixel format. In the later reconstructions only the central part was reconstructed ($64 \times 64 \times 64$ pixels), with one monomer in the center. Comparison showed that the latter reconstructions had more structural detail in the 2–5 nm range. Moreover, the errors between input projections and projections calculated from the reconstruction were lower (always under 10%). Overcorrection factors [23] of 1.5 for the first 10 iterations and 1.1 for the next 10–20 gave the best reconstructions.

(5) The reconstruction was high-pass and low-pass filtered with a gaussian mask to suppress noise details larger than 16 nm and smaller than 2.5 nm, respectively.

(6) The reconstructions from the three tilt-series were combined. Since from each of the three tilt-series the up- and the down-oriented monomers were reconstructed separately, actually six reconstructions were combined.

Results

Preparation and analysis of two-dimensional crystals

Fig. 1 shows a silver stained SDS-gel of the Photosystem I preparation. The bands are labelled according to Ref. 9. In this work, the N-terminal amino acid sequence of each band in the gel was determined and compared with the gene-derived sequence. Our preparation contains the following subunits: psaA, psaB, psaC, psaD, psaF and psaJ. The band labelled X is an impurity, the subunits psaE, psaK and psaM could not be detected. The difference in subunit composition

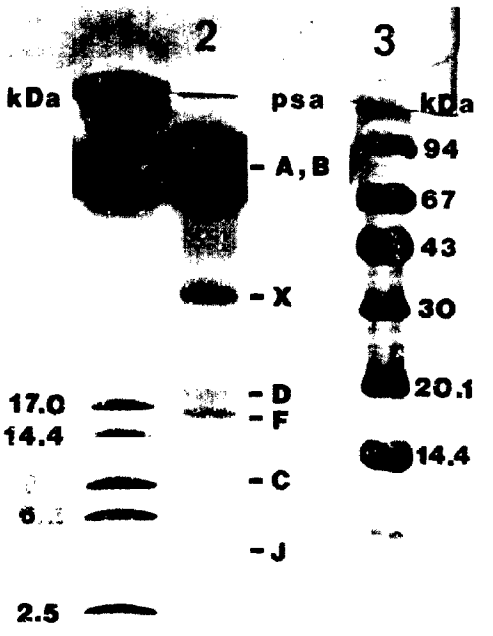

Fig. 1. Silver stained SDS-gel of the PS I preparation. Lane 1: low molecular weight marker; lane 2: PS I preparation (1 μl containing 0.15 μg chlorophyll was applied); lane 3: high molecular weight marker.

might be due to the fact that our preparation contains PS I monomers, whereas in Ref. 9 trimers are observed. A smaller number of subunits in the monomer was also observed in Ref. 17.

Two-dimensional crystals of PS I were obtained by incubating aliquots of sample with phospholipase A_2 or lipase and Bio-Beads at 4°C. The crystalline areas were optimal after 5–10 days. If phospholipase A_2 was omitted, the crystallization process took longer and the packing in the crystalline arrays was not as good. Addition of 5 mM Ca^{2+}, which should stimulate the phospholipase A_2 activity, did not effect the crystal growth. Therefore, it was omitted in most cases. If phospholipase or lipase were added in 10 to 100-times larger quantities crystals disappeared once they were formed. These observations possibly indicate the existence of a narrow region of lipid:protein ratios where crystals can exist. Crystals were also obtained after 14 days by dialysis against 2 mM $MgSO_4$ and phospholipase A_2 treatment. No crystals of any preparation could be obtained at room temperature. Crystals of PS I preparations solubilized with octyl glucoside contained substantial amounts of ATP synthase, which aggregated in non-crystalline areas. But if sulfobetain 12 was used in the solubilization step, both the final preparation and the crystals were almost free of ATP

synthase. The quality of the crystalline arrays, however, was not substantially improved.

Usually crystalline double-layers were observed, caused by a collapse of a vesicle crystal (Fig. 2), but monolayers were also frequent. The largest crystals measured 0.5 × 1 μm and contained about 3000 monomers in one layer. Optical diffraction of the double-layer crystals showed that the stacking of the layers was not in register: both layers were randomly orientated in respect to each other (Fig. 2A). This gives us the opportunity to process the layers separately by the correlation averaging method [22]. In this procedure a Fourier-peak filtered image of each layer is used as a reference in the actual correlation averaging step. Fig. 3A,B show the results of the processing. Both layers show rows of monomers with a slightly elongated shape. In one layer the monomers appear all similarly stained (Fig. 3B), whereas in the other one the monomers appear differently embedded in the stain (Fig. 3A). The homogeneously stained layer is presumably the one attached to the carbon support. To evaluate the crystal packing, the sums of Fig. 3A,B were Fourier transformed (Fig. 3C,D). In the transform of the evenly stained layer (Fig. 3D) the odd reflections on the vertical axis are missing or very weak, indicating a screw axis in the plane of the crystal [26]. In the transform of the other layer (Fig. 3C) this screw axis does not be seen, because uneven staining causes the monomers look different. Each layer of a crystal has a rectangular unit cell with dimensions of 16.0 (±0.3) × 15.0 (±0.14) nm (S.D.; average of 8 crystals); the angle between the axes was 89.6° (±0.7°). The packing of the crystals was $p12_1$ (equivalent to pg) [26]. This means that the unit cell contains two monomers and that the monomers are oriented up and down in alternating rows with respect to the plane of the crystal. The transform in Fig. 3D shows many strong spots, such as a (7,3) spot corresponding to a resolution of 1.8 nm. Higher order spots (the (1,10), (4,9), (10,1) and the (7,7) spots) are related to structural details with a resolution of about 1.5–1.8 nm, but their amplitudes are much weaker.

Metal shadowing of crystals

In transmission electron microscopy, two-dimensional projections are obtained in which all details are superimposed and seen with the same 'sharpness', irrespective of their height in the vertical direction.

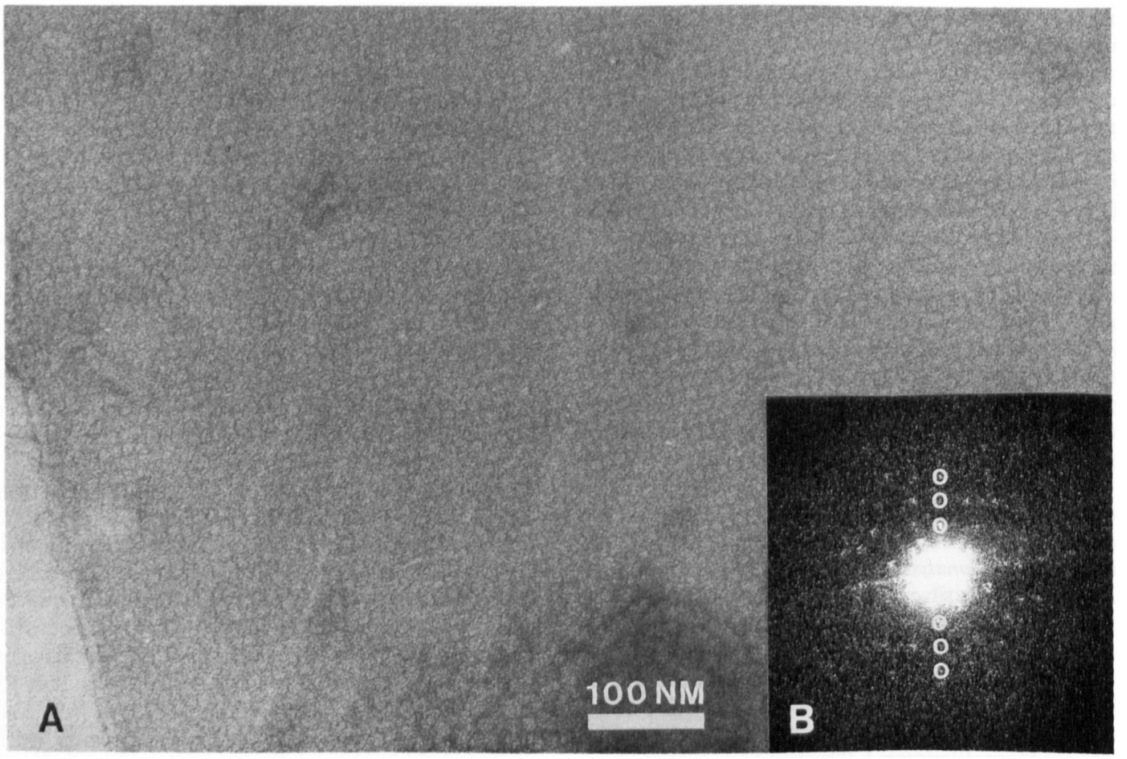

Fig. 2. (A) Part of an original electron micrograph showing a collapsed membrane crystal of Photosystem I used for the analysis. The crystal was negatively stained with a 1% solution of uranyl acetate; (B) optical diffraction pattern from (A) indicates multiple spots from both layers in different rotational positions. One row of spots has been indicated; the outer fourth-order spots indicate a resolution of 4 nm before processing.

Three-dimensional information can be acquired in two ways. One way is to decorate the object by evaporating with a heavy metal. Knowing the angle between the sample and the evaporation source, this shadowing technique gives information of the surface relief. We applied unidirectional shadowing with platinum to the PS I crystals. One large shadowed crystal (Fig. 4A) was processed by correlation averaging. Fig. 4B shows the final sum of the aligned fragments. The contours of the monomers, which can be easily recognized in negatively stained specimens (Fig. 3), are difficult to discern in the shadowed crystal. But the diffraction pattern (Fig. 4C), which is the Fourier-transformation of Fig. 4B, indicates that the rows of monomers run from top

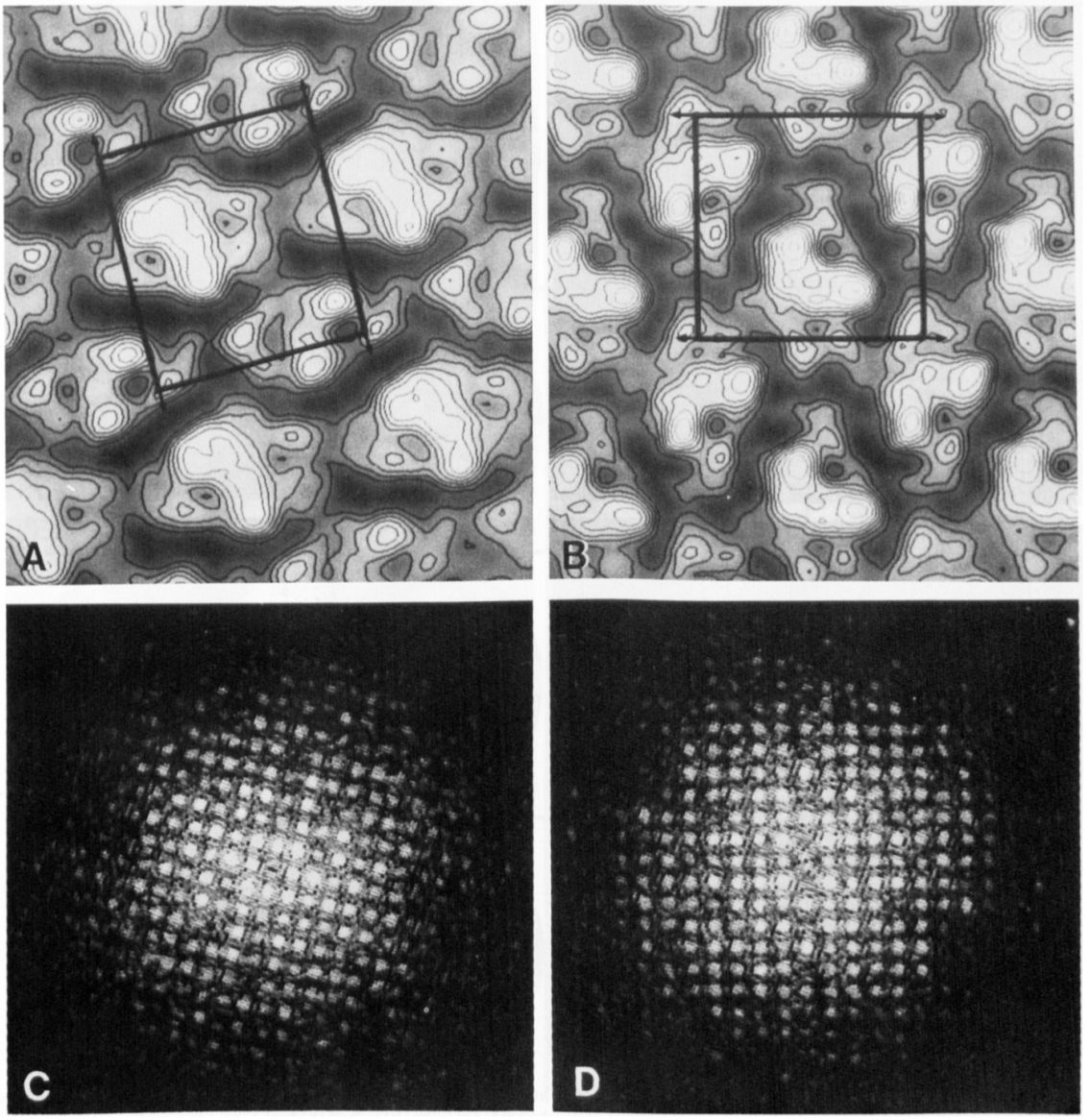

Fig. 3. Image analysis of the two layers of a collapsed vesicle crystal. (A) the result of correlation averaging: the sum of the best 750 128×128 pixel fragments (out of 2000) of one layer. For representation, the sum has been interpolated to a 768×768 pixel format and contoured with equidistant contour lines. The inner part of about 500×500 pixels is shown; (B) the final sum of the other layer, processed as for (A); (C) calculated diffraction pattern (Fourier transform) of the sum of (A); (D) calculated diffraction pattern of (B). The unit cell has been indicated for both layers with dimensions of 16×15 nm.

to bottom, as in Fig. 3B. In one type of row there are dark metal depositions of 4 × 6 nm ('ridges', see Fig. 4D), which are absent in the other type of row (marked with asterices). From the shadow length it can be estimated that the height of a ridge is about 3 nm. This means that at one side the monomer clearly extends the membrane. The shadowing pattern of the upside-down rows indicates that on the other side the monomers extend the membrane by about 1 nm, see Fig. 4D).

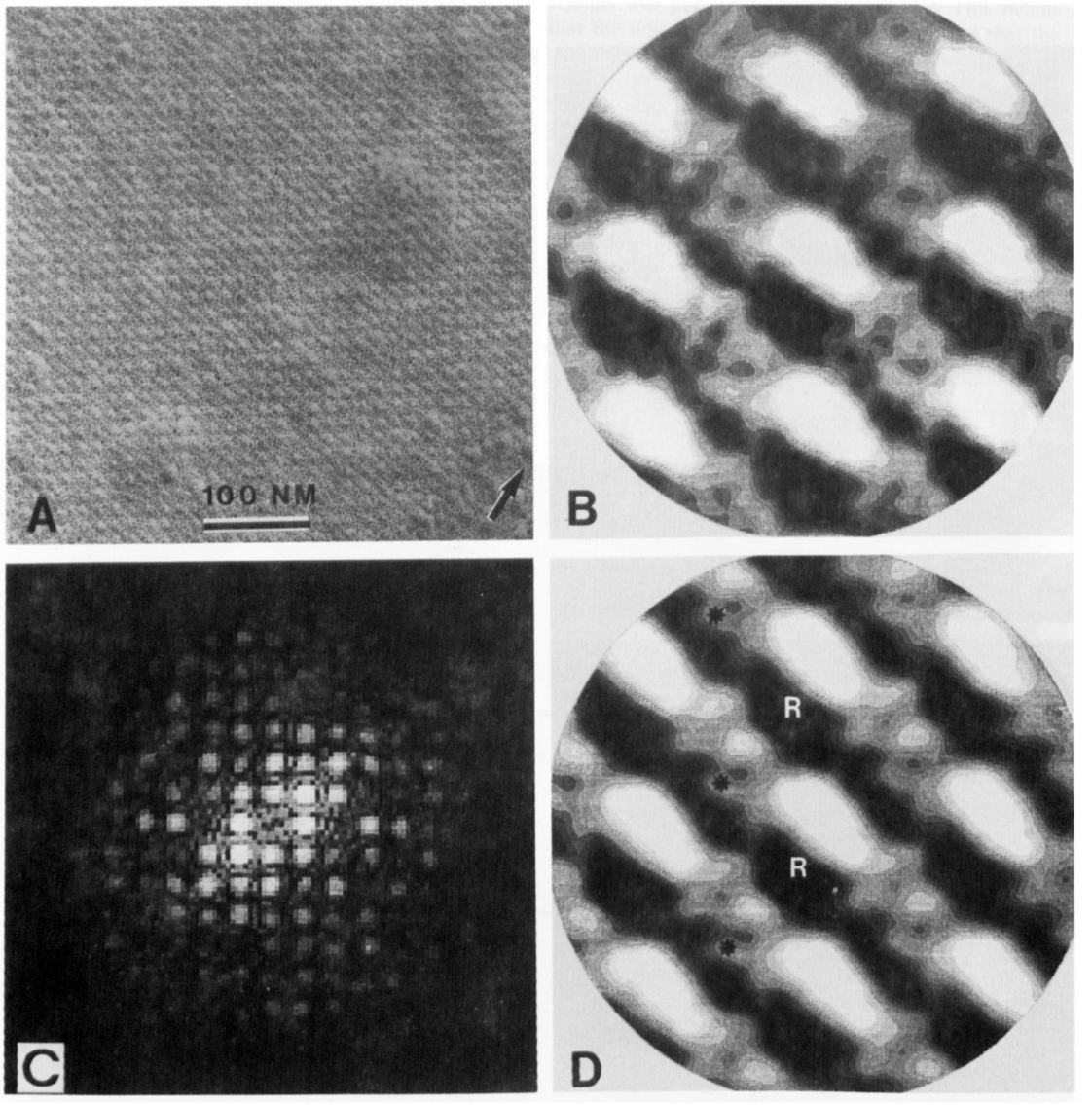

Fig. 4. (A) A PS I crystal, unidirectional shadowed with platinum from an angle of 25° after drying on the grid. The direction of the shadow is indicated by an arrow, metal deposits are dark, uncovered crystal parts (shadows) are light; (B) sum of the best 128 × 128 pixel fragments after the correlation averaging step; (C) Fourier transform of the sum of B; (D) Fourier-peak filtered image of (B). The contours of the individual monomers cannot be discerned, but the diffraction pattern of (B) indicates that monomers are oriented as in Fig. 3A. The positions of a ridge (R) of about 4 × 6 nm, which extends about 3 nm above the plane of the crystal, have been indicated. Asterices indicate the equivalent positions in one neighboring row where the monomers are oriented upside-down. At these positions, only smaller extensions of about 1 nm can be seen. The diameter of the circular mask is 50.6 nm.

Three-dimensional reconstruction

More detailed three-dimensional information can be obtained after tilting the specimen in the microscope and calculating a three-dimensional structure from the tilted projections. We have applied a tomographic ('direct space') reconstruction method to calculate the PS I structure. Three tilt series were recorded from mono-layer crystals. The first one was comprised of 15 images running from −33.5° to +56.5°, the second one of 18 images from −50° to +52° and the third one of 14 images from −40.5° to +51°. They were processed in six subsequent steps as indicated in the 'Methods' section. In the first step all 47 different projections were filtered by correlation averaging, with a Fourier-peak filtered crystal part as the first reference. The final resolution in the 47 filtered projections varied

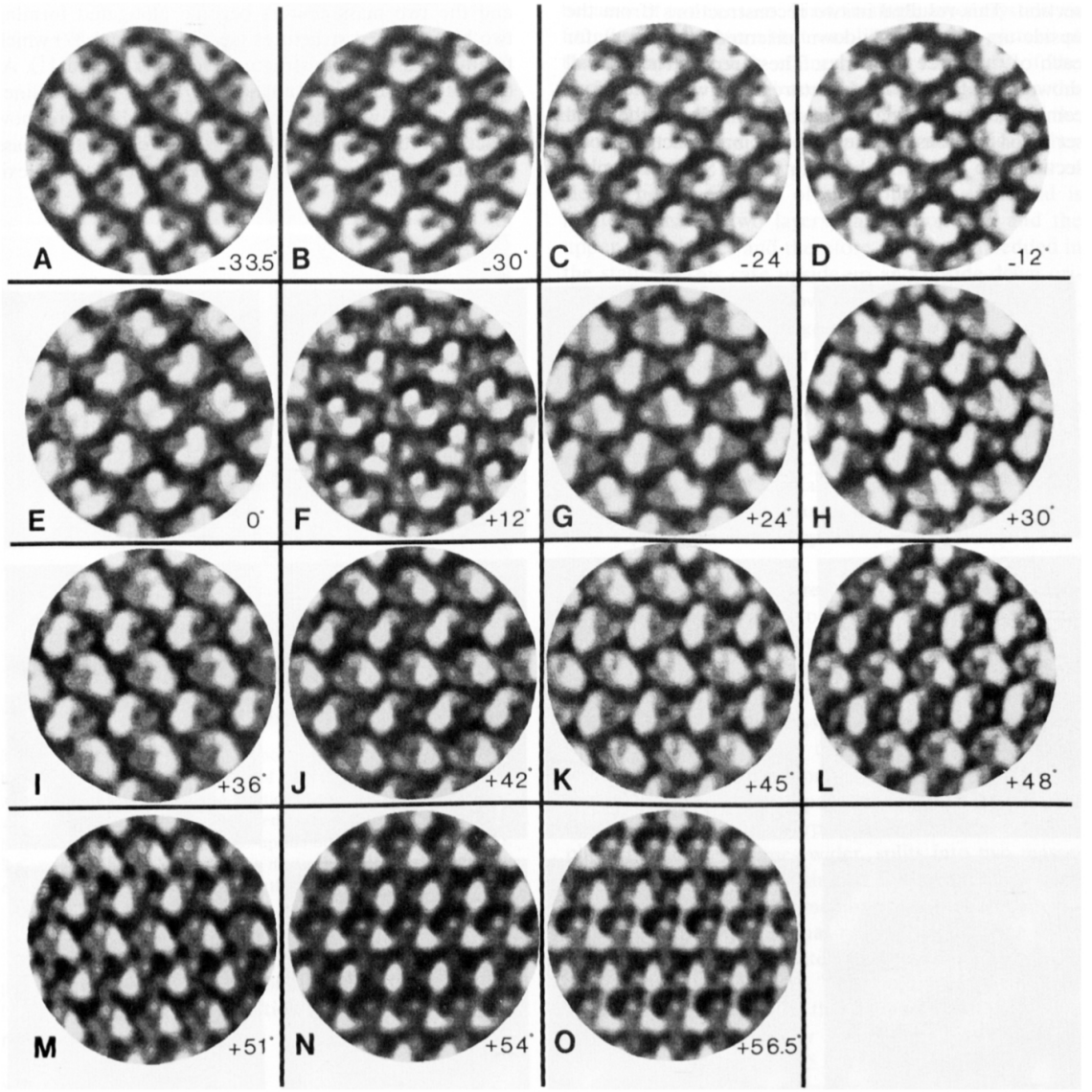

Fig. 5. The tilted projected structure of a mono-layered PS I crystal from a single tilt-axis series of 15 micrographs. Each image is the sum of the best 450 aligned crystal fragments from the best underfocussed part of the crystal. The tilt axis is from top to bottom and by coincidence, one crystal axis is running parallel to the tilt axis with a deviation of less than 1°. The respective tilt angles have been indicated. All images have been shifted to a common origin. For presentation, the 128×128 pixel sums were interpolated to a 384×384 format and windowed with a circular mask with a diameter of 365 pixels, which is equivalent to 50.6 nm.

between 2 and 2.5 nm. Fig. 5 shows the filtered projections of the first tilt series. By coincidence, one crystal axis is running parallel to the tilt axis (which is vertically oriented in Fig. 5) and the shortening of the unit cell upon tilting occurs only in the horizontal direction. The subsequent shortening of the monomers can be clearly followed going from 0° (Fig. 5E) to +56.5° (Fig. 5O).

The next steps of the reconstruction scheme were carried out as described in the Materials and Methods section. This resulted in two reconstructions (from the upside-up- and upside-down oriented monomer) for each of the three tilt series. These reconstructions all showed similarly shaped features and were therefore combined to one final reconstruction. From the total set of 64 sections a gallery of the inner sections (odd sections No 21–43) is shown in Fig. 6. Section number 21 is the second one from the top of the model of Fig. 7. The top of the model represents presumably the stromal side of PS I (see Discussion). In section 21 a central mass with only three contour lines can be seen. Going from top to bottom the number of contour lines increases (indicating a higher mass density in the center of the protein) and the central mass splits into two separate mass centers which can be recognized best in sections 31 and 33. Going further to the bottom of the molecule the number of contour lines decreases again and the two mass centers become elongated forming two bean shaped structures (sections 35 and 37) which finally close to a ring structure (sections 39 and 41). At the bottom (section 43) again only three contour lines can be seen with two mass centers which are now placed at different positions compared to the mass centers in sections 29–31. A three-dimensional plexi-

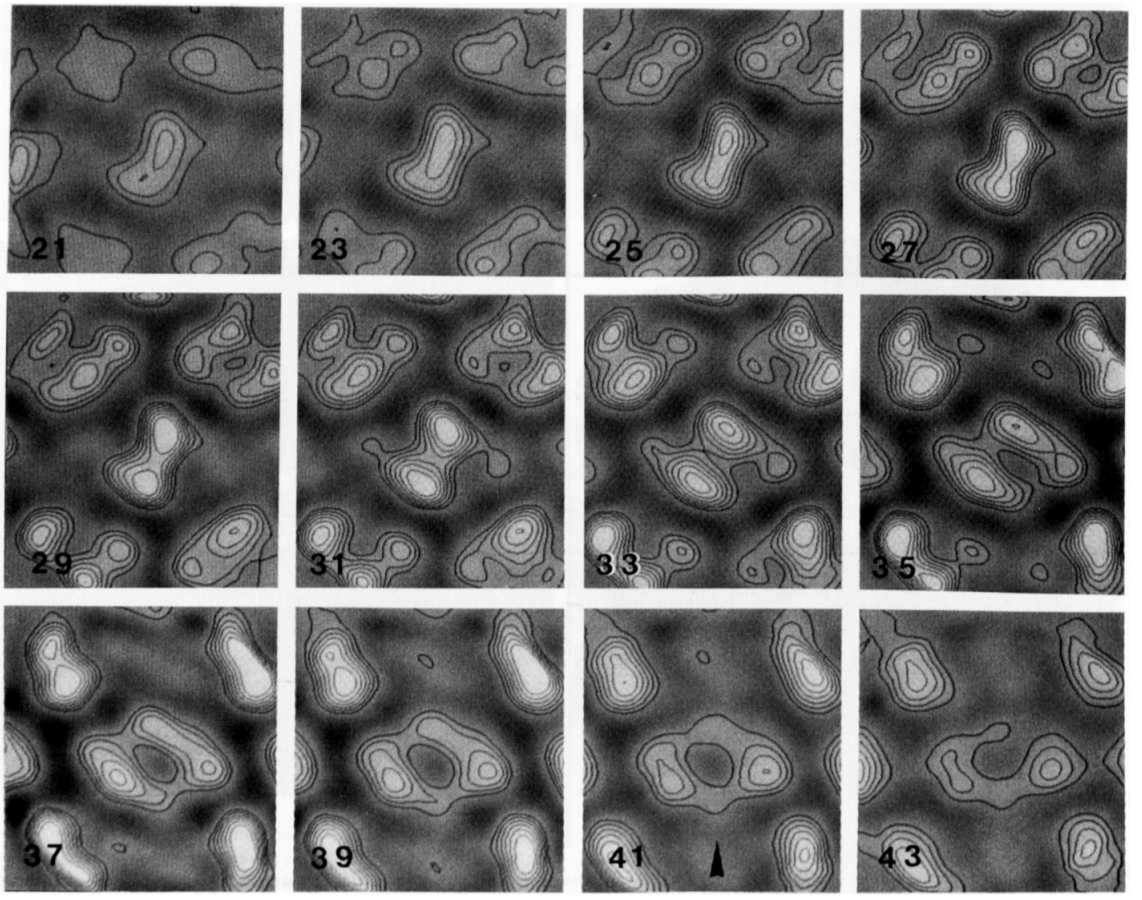

Fig. 6. The three-dimensional reconstruction of PS I, represented as a gallery of sections 0.42 nm apart through the reconstructed object. The sections are parallel to the plane of the crystal. The upper sections are from the stromal side, the lower sections from the lumenal side of PS I. The section numbers have been indicated, the lowest section is the second one from the top of the model in Fig. 7.

Fig. 7. Two views of a perspex model for the three-dimensional shape of PS I. The model consists of 24 sections of 0.42 nm parallel to the plane of the crystal. The location of the 5 nm thick membrane has been indicated and was deduced from differences in height of the reconstructed upside-up- and upside-down-oriented monomers. The arrow indicates the part of the monomer which is closest to the center of the trimeric PS I particles, the same place is also marked in Fig. 6.

glass model made from sections 20–43 is shown in Fig. 7. The most probable position of the membrane is indicated (see Discussion).

Discussion

Two-dimensional projection

In this study the structure of PS I was investigated by electron microscopy of negatively stained crystals. In the first step image processing on the two-dimensional projection was carried out. A resolution of 1.5–1.8 nm was achieved, as determined from the diffraction pattern. This is close to the limit of the negative staining procedure. Usually, the crystals form double layers. Image processing of these layers was carried out separately and it was found that one layer is very homogeneously stained whereas the other one is inhomogeneously stained. We assume that the more homogeneously stained layer is closer to the carbon support because of two reasons. First, in single layer crystals we found a stain pattern that was like the stain pattern of the inhomogeneously stained layer. Obviously, if the particles of the crystal are not fully embedded in the stain, they should show a different appearance for the upside-up- and upside-down oriented molecules if they are asymmetric in their shape parallel to the axis of view. The lower layer of the double-layer crystal is located between two layers, the carbon film and the upper crystal layer and therefore is better embedded in the stain. In this case upside-up and upside-down oriented molecules will show the same staining profile. Second, the average image of the homogeneous layer indicates a slightly higher resolution than the average image of the more inhomogeneous one. The layer with the higher resolution is presumably located directly on the carbon film, which is relatively smooth. The layer with the lower resolution is located on the lower crystalline layer which is relatively rough (the layers are not in register). This causes disordering in the crystalline packing followed by a loss of resolution.

Three-dimensional structure

The metal-shadowing of the crystals indicates that the molecule projects about 3 nm out of one side of the membrane and 1 nm at the other side. This is in accordance to the conclusions from the inhomogeneous staining of the crystals. The three-dimensional reconstruction from the different tilt series provide more detailed information. On the top side of the molecule there is a compact elongated mass. Passing through the molecule perpendicular to the membrane plane the mass becomes wider, splits into two masses and finally forms a ring-shaped structure at the other side. The location of the membrane cannot be deduced from the three-dimensional reconstruction. The shadowing experiments indicate that the ridge extends the membrane 3 nm (Fig. 4). This is equivalent to 7 sections of the model. On the lumenal side the model sticks out about 1 nm or 2 sections. The membrane bilayer is supposed to be 5 nm (about 12 sections). The model includes 24 sections or 10 nm. Thus, there is some discrepancy between the shadowing experiments (21 sections inferred) and the reconstruction (24 sections). However, the resolution of the reconstruction perpendicular to the membrane is only about 4 nm,

i.e., it is much lower than in the membrane plane. This is a result from the limited maximum angles of the three tilt series. It was shown that each pixel becomes elongated in the z-direction if a reconstruction is based on projections over a limited tilt angle [27]. This causes overlapping of the pixel information in the z-direction. The image information becomes blurred out in this direction. Thus, the localization of the membrane can only be roughly (with 1–2 nm accuracy) indicated. In the model of Fig. 7 the membrane is situated between sections 30 and 41.

The volume of the molecule as depicted in Fig. 7 is about 310 nm^3. With a density of 1.38 g cm^{-3} a molecular mass of about 260 kDa is calculated. Based on the sequence derived molecular masses of the subunits, a molecular mass of 232 kDa is calculated. Since PS I contains about 60 Chl, the total mass is about 292 kDa in accordance with the estimation from the volume of the molecule. If a slightly higher volume was taken (350 nm^3 instead of 310 nm^3) the difference resulted in a smaller additional mass in the ring area, extending from section 43 to 48 (i.e., about 2.7 nm with a volume of 27 nm^3). Because of the limited resolution in the z-direction, we cannot finally decide whether this extension is real or an artifact. The information of trimeric particles in side view position (see below), which points to a maximal height of less than 10 nm indicates, however, that the extension is most likely an artifact.

Orientation of PS I in vivo

It is of interest to discuss the features of the model and the implications for the subunit organization of PS I, even at the low resolution level obtained. The three-dimensional reconstruction does not give evidence in which manner the PS I is oriented *in vivo*. However, some arguments lead to the conclusion that the top of the model of Fig. 7 is on the stromal side of the membrane *in vivo*. On the top side, the model shows a ridge in the center. This ridge includes 10 sections (about 4 nm). The ridge is the feature of the reconstruction that sticks out the farthest from the plane of the membrane. This can be seen by comparing sections on both sides of the reconstruction (Fig. 6). In section 27 the ridge in the center of the image is contoured by six contour lines, indicating a high density. In the top of the image the upside-down oriented monomers are contoured by only four lines. In section 43 the ridge in the molecules in the top left and right positions is contoured with more contour lines. Thus, it sticks out farther from the plane of crystal than the part of the reconstruction with the central indentation.

Based on earlier results with crosslinking experiments [28,29] we suppose that the hydrophilic subunits, psaC, psaD and psaE (which is not present in this preparation) are located on the stromal side of the membrane and that these subunits form the ridge.

That the ridge is in a central position on top of the membrane-embedded PS I part is understandable, because psaC contains two iron-sulfur clusters, which must accept electrons from another iron-sulfur cluster which is bound at the interface between the large subunits psaA and psaB. A central position is also understandable because psaC is essential for PS I stability [30]. On the lumenal side there is only one extrinsic subunit, psaF, which binds cytochrome *c*-553 and has a mass of 15 kDa [9].

On the bottom (lumenal side) of the model there is a central indentation of about 3 nm in diameter and in depth (Fig. 6,7). This separates the reconstruction in two halves of about the same shape. Since the lumenal side sticks out the membrane by only about 1 nm, this means that the separation occurs also within the membrane. The two large subunits psaA and psaB (without chlorophylls) contribute to more than 50% of the mass of PS I. They both have 11 hydrophobic amino acid stretches, supposed to be buried as α-helices in the membrane [31]. It is likely that the two separated halves of the model on the lumenal side coincide with the positions of the large subunits. Other possibilities for the position of the large subunits can almost be excluded. The membrane-embedded α-helices of psaA and psaB are very hydrophobic and it is not likely that negative stain will separate them. Sections 37 and 39 (Fig. 6) are on the level were the separation of the two halves is the clearest. The contour lines indicate that both halves have about the same area. But in addition to psaA and psaB other subunits will also contribute to the shape and form; thus, it is not surprising that both halves are not exactly the same. One particular detail seen in one half is a protrusion (see arrows in Fig. 6 and 7) that forms the center of PS I in the trimeric arrangement of the monomers.

The central indentation is visible because the negative stain penetrates into the part of the PS I structure that is embedded within the membrane. This is only possible if the protein surface is locally more hydrophilic. Additional insertion of hydrophilic loops of the psaA and psaB polypeptide chains into the center of the PS I structure on lumenal side could realize this situation. But although the indentation is about 3 nm in width and depth, psaA and psaB must be partly in close contact possibly by hydrophobic interaction of leucine side-chains of two helices [32]. This contact between psaA and psaB must be somewhere in the center of the model. It is evident that a much higher resolution in the reconstruction will be necessary to observe such details in the PS I model. Such higher resolution could, in principle, be obtained by cryo-electron microscopy of sucrose-embedded larger-sized crystals [18].

Comparison of monomers and trimers from PS I

PS I complexes have been isolated as monomers from many sources, but also as stable monomeric and trimeric particles from several cyanobacteria, such as *Synechococcus* sp. [10,11], *Phormidium laminosum* [12] and *Synechocystis* PCC 6803 [33]. In our crystals it is obvious that PS I is in the monomeric form only, possibly because our isolation procedure favors the extraction of monomers. The features of the projected monomers, as seen in the *Synechococcus* crystals and single trimeric particles [11], cannot be correlated very well. However, recently we analyzed *Synechocystis* trimers by single particle averaging with a higher resolution and now the features from the monomers of crystals and trimers look more similar, even in the finest details (unpublished results).

Analysis of side views of trimers gives additional information about the shape of PS I vertical to the membrane. Negative staining induces aggregation of trimers in side view position. Although the trimers come close together when they aggregate, there remains always a small stain-filled gap between two adjacent monomers [10,11]. Originally, it seemed that all gaps from a string had the same width [10]. However, more recent images (unpublished results) showed clearly the alternation of smaller and larger gaps in aggregated side views. The larger gaps appear when two trimers aggregate 'face-to-face' into so-called double trimers, the smaller gaps appear between the double trimers. From the side view aggregation behavior it can be concluded that both sides of a trimer are dissimilar; on one side there must be a protrusion of maximally 4 nm that hinders a closer packing. X-ray diffraction studies showed that three-dimensional PS I crystals have a unit cell dimension of 16.7 nm in the direction that coincides with the staggering of double trimers [14]. Thus, the width of one monomer is at least 8.4 nm. But if the double trimers would intercalate as far as possible, a width of almost 10 nm could be expected.

Comparison with literature data

Previously, two-dimensional crystals of PS I from *Synechococcus* sp. have been obtained by Ford et al. [13] by reconstitution in phospholipid bilayers. Their method and conditions differed slightly from ours. In the reconstitution step, detergent was removed by dialysis instead of absorption with Bio-Beads. In the crystallization experiments of Ford et al. the detergent octyl β-D-thioglucopyranoside was used; no crystals could be obtained with dodecyl maltoside, although this detergent gave very good crystals in our crystallization experiments. The crystal symmetry for a single layer ($p12_1$) was the same, but the unit cell dimensions (14.5×14.5 nm) were slightly smaller than ours (16×15 nm). Our crystals are bigger and the slightly higher resolution in the two-dimensional projection (1.5–1.8 nm) results in better resolved details. Six maxima and two minima in densities of the staining profile of a monomer can be observed in the two-dimensional projection (Fig. 3). Three-dimensional information was obtained by Ford et al. [13] by metal shadowing. From these results a model was deduced showing a ridge at one side of the molecule and a central indentation on the other side. The three-dimensional reconstruction presented here gives the same shape of the molecule and additionally reveals more details because of the higher resolution.

Acknowledgements

We wish to thank Professor Dr. E.F.J van Bruggen for general support, Prof. Dr. H.T. Witt for the *Synechococcus* cells, Dr. W. Keegstra for his help with computer image analysis, Dr. P. Fromme and Petra Jakow for the SDS-gel electrophoresis, Dr. J.P. Dekker for stimulating discussions, Mr. S.L.S. Kwa for recording fluorescence spectra and Mr. K. Gilissen for photography. The research of B.B. has been made possible in part by a grant from the Commission of the European Communities as part of the Biotechnology program and was further supported by the Landesgraduiertenförderung of Baden-Württemberg. E.J.B. is supported by the Royal Netherlands Academy of Arts and Sciences.

References

1 Bryant, D. (1991) in Current Topics in Photosynthesis, Vol. 11 (Barber, J., ed.), Elsevier, Amsterdam.
2 Margulies, M.M. (1989) Plant Sci. 64, 1–13.
3 Lagoutte, B. and Mathis, P. (1989) Photochem. Photobiol. 49, 833–844.
4 Scheller, H.V. and Moller, B.L. (1990) Physiol. Plant. 78, 484–494.
5 Newman, P.J. and Sherman, L.A. (1978) Biochim. Biophys. Acta 503, 343–361.
6 Nakayama, K., Yamaoka, T. and Katoh, S. (1979) Plant Cell Physiol. 20, 1565–1565.
7 Lundell, D.J., Glazer, A.N., Melis, A. and Malkin, R. (1985) J. Biol. Chem. 260, 646–654.
8 Rögner, M., Mühlenhoff, U., Boekema, E.J. and Witt, H.T. (1989) Biochim. Biophys. Acta 1015, 415–424.
9 Mühlenhoff, U., Witt, H.T. and Hermann, R. (1992) Nucleic Acids Res., in press.
10 Boekema, E.J., Dekker, J.P., Van Heel, M.G., Rögner, M., Saenger, W., Witt, I. and Witt, H.T. (1987) FEBS Lett. 217, 283–286.
11 Boekema, E.J., Dekker, J.P., Rögner, M., Witt, I., Witt, H.T. and Van Heel, M. (1989) Biochim. Biophys. Acta 974, 81–87.
12 Ford, R.C. and Holzenburg, A. (1988) EMBO J. 7, 2287–2293.
13 Ford, R.C., Hefti, A. and Engel, A. (1990) EMBO J. 9, 3067–3075.
14 Witt, I., Witt, H.T., Di Fiore, D., Rögner, M., Hinrichs, W., Saenger, W., Granzin, J., Betzel, Ch. and Dauter, Z. (1988) Ber. Bunsenges. Phys. Chem. 92, 1503–1506.
15 Ford, R.C., Picot, D. and Garavito, M. (1987) EMBO J. 6, 1581–1585.

16 Reilly, P. and Nelson, N. (1988) Photosynth. Res. 19, 73–84.
17 Almog, O., Shoham, G., Michaeli, D. and Nechushtai, R. (1991) Proc. Natl. Acad. Sci. USA 88, 5312–5316.
18 Henderson, R., Baldwin, J.M., Ceska, T.A., Zemlin, F., Beckmann, E. and Downing, K.H. (1990) J. Mol. Biol. 213, 899–929.
19 Boekema, E.J. (1990) Electron Microsc. Rev. 3, 87–96.
20 Schatz, G.H. and Witt, H.T. (1984) Photobiochem. Photobiophys. 7, 1–14.
21 Saxton, W.O and Baumeister, W. (1982) J. Microsc. 127, 127–138.
22 Kessel, M., Radermacher, M. and Frank, J. (1985) J. Microsc. 139, 63–74.
23 Boekema, E.J., Van Heel, M.G. and Van Bruggen, E.F.J. (1984) Biochim. Biophys. Acta 787, 19–26.
24 Boekema, E.J., Van Heel, M.G. and Van Bruggen, E.F.J. (198) Methods Enzymol. 126, 344–353.
25 Shaw, P.J. and Hills, G.J. (1981) Micron 12, 279–282.
26 Hovmöller, S. (1986) in Techniques for the analysis of membrane proteins (Ragan, C.I. and Cherry, R.J., eds.), Chapman & Hall, London.
27 Radermacher, M. (1988) J. Electr. Microsc. Techn. 9, 359–394.
28 Andersen, B., Koch, B., Scheller, H.V., Okkels, J.S. and Moller, B.L. (1989) in Current Research in Photosynthesis (Baltscheffsky, M., ed.), Vol. II, pp. 671–674.
29 Zhao, J., Warren, P.V., Li, N., Bryant, D.A. and Golbeck, J.H. (1990) FEBS Lett. 276, 175–180.
30 Takahashi, Y., Goldschmidt-Clermont, M., Soen, S.-Y., Franzen, L.G. and Rochaix, J.-D. (1991) EMBO J. 10, 2033–2040.
31 Golbeck, J.H. (1987) Biochim. Biophys. Acta 895, 167–204.
32 Webber, A.N. and Malkin, R. (1990) FEBS Lett. 264, 1–4.
33 Rögner, M., Nixon, P.J. and Diner, B. (1990) J. Biol. Chem. 265, 6189–6196.